physica status solidi rrl
www.pss-rapid.com

Exciton–Polaritons in $CsPbBr_3$ Crystals Revealed by Optical Reflectivity in High Magnetic Fields and Two-Photon Spectroscopy

Dmitri R. Yakovlev, Scott A. Crooker, Marina A. Semina, Janina Rautert, Johannes Mund, Dmitry N. Dirin, Maksym V. Kovalenko, and Manfred Bayer*

Cesium lead bromide ($CsPbBr_3$) is a representative material of the emerging class of lead halide perovskite semiconductors that possess remarkable optoelectronic properties. Its optical properties in the vicinity of the bandgap energy are greatly contributed by excitons, which form exciton polaritons due to strong light–matter interactions. Exciton–polaritons in solution-grown $CsPbBr_3$ crystals are examined by means of circularly polarized reflection spectroscopy measured in high magnetic fields up to 60 T. The excited 2P exciton state is measured by two-photon absorption. Comprehensive modeling and analysis provides detailed quantitative information about the exciton–polariton parameters: exciton binding energy of 32.5 meV, oscillator strength characterized by longitudinal–transverse splitting of 5.3 meV, damping of 6.7 meV, reduced exciton mass of $0.18m_0$, exciton diamagnetic shift of 1.6 μeV T^{-2}, and exciton Landé factor $g_X = +2.35$. It is shown that the exciton states can be described within a hydrogen-like model with an effective dielectric constant of 8.7. From the measured exciton longitudinal–transverse splitting, Kane energy of $E_P = 15$ eV is evaluated, which is in reasonable agreement with values of 11.8–12.5 eV derived from the carrier effective masses.

1. Introduction

Cesium lead bromide ($CsPbBr_3$) is a fully inorganic member of the large family of lead halide perovskite semiconductors.[1,2] This material delivers an outstanding combination of optoelectronic properties, such as long charge carrier diffusion lengths up to 1.3 μm,[3] high carrier mobilities (10–181 $cm^2V^{-1}s^{-1}$),[3,4] low densities of carrier trap states (3.9×10^{10} cm^{-3}) despite a large density of point defects,[3] and small carrier effective masses ($0.17m_0 - 0.26m_0$) combined with large polarons.[5] $CsPbBr_3$ has been recently applied to the fabrication of perovskite solar cells,[6,7] sensitive visible light detectors,[8] and high-energy detectors.[9,10] Fully inorganic $CsPbBr_3$ exhibits higher stability against elevated temperatures and polar solvents compared to analogous lead halide perovskites that incorporate organic cations, for example, methyl ammonium (MA) lead bromide. In applications for hard radiation detection, $CsPbBr_3$ is indispensable as it is the only lead halide perovskite that can operate under the high bias required for efficient extraction of charge carriers.[10]

Optical properties of semiconductors in the vicinity of the bandgap energy are controlled by excitons, making knowledge of the exciton parameters of great importance for optoelectronics. $CsPbBr_3$ is a model material for the class of lead halide perovskite semiconductors. It is widely studied experimentally and theoretically, with initial papers on exciton properties dating back to 1978.[11–14] Light–matter interactions are quite strong in

D. R. Yakovlev, J. Rautert, J. Mund, M. Bayer
Experimentelle Physik 2
Technische Universität Dortmund
44227 Dortmund, Germany
E-mail: dmitri.yakovlev@tu-dortmund.de

S. A. Crooker
National High Magnetic Field Laboratory
Los Alamos National Lab
Los Alamos, NM 87545, USA

The ORCID identification number(s) for the author(s) of this article can be found under https://doi.org/10.1002/pssr.202300407.

DOI: 10.1002/pssr.202300407

M. A. Semina
Ioffe Institute
Russian Academy of Sciences
194021 St. Petersburg, Russia

D. N. Dirin, M. V. Kovalenko
Laboratory of Inorganic Chemistry
Department of Chemistry and Applied Biosciences
ETH Zürich
CH-8093 Zürich, Switzerland

D. N. Dirin, M. V. Kovalenko
Laboratory for Thin Films and Photovoltaics
Department of Advanced Materials and Surfaces
Empa - Swiss Federal Laboratories for Materials Science and Technology
CH-8600 Dübendorf, Switzerland

$CsPbBr_3$,[15–18] which results in a pronounced resonance in optical reflectivity and absorption spectra in the vicinity of the bandgap. Following the classic formulations of electromagnetic waves interacting with exciton oscillators in semiconductors, these optical resonances are modeled in the context of "exciton–polariton" quasiparticles.[19,20] Exciton–polaritons are a fundamental manifestation of light–matter interactions in all bulk semiconductors with direct bandgaps, and detailed analyses of their associated resonances in optical spectra provide tremendous insight into the underlying exciton parameters in the material (masses, binding energies, damping, longitudinal–transverse splitting, etc). We note that in recent years considerable attention has focused on the related topic of microcavity exciton–polaritons,[21] wherein light–matter couplings can be further enhanced and anticrossing between cavity and exciton modes can be clearly observed. However, the fundamental exciton–polariton quasiparticles exist even in the absence of any additional cavity.

Magneto-optical methods are powerful tools to measure exciton parameters in semiconductors.[19,22–24] Exciton binding energies can be evaluated from the diamagnetic shift of the 1S exciton state in magnetic fields and/or from the observation of excited exciton states (2S, 3S, etc.), which gain oscillator strength and become increasingly visible in high fields. In both cases, the exciton linewidth is a critical parameter for the evaluation accuracy, which in turn is improved in high magnetic fields. Magneto-optical studies in high magnetic fields of 45–150 T were successfully used for investigation of lead halide perovskite semiconductors.[25–35] Most studies to date were made on polycrystalline films with rather broad exciton lines, and results on single crystals with small inhomogeneous broadening of the excitons are available only for $MAPbBr_3$[35] and $MAPbI_3$.[32]

For $CsPbBr_3$ films, measurements in magnetic fields up to 150 T indicate an exciton binding (Rydberg) energy of 33 meV and a reduced exciton mass of $\mu = 0.126m_0$.[31] Note that earlier and not very detailed reports inferred exciton binding energies of 37 meV[13] and 34 meV.[36] Importantly, however, $CsPbBr_3$ has a rich spectrum of optical phonons with energies ranging from 4 to 25 meV,[37,38] values which are close to, but smaller than, the exciton binding energy. It is generally in the energy range of the optical phonons where the magnitude of the energy-dependent dielectric constant $\varepsilon(\omega)$ varies significantly between its stationary (i.e., zero-frequency) value (ε_s) and its value in the high-frequency limit (ε_∞). This fact provides two aspects for the exciton properties and calculation of its parameters. The first one is that phenomenologically the exciton energies are often described in the framework of a hydrogen-like model, but with an effective dielectric constant ε_{eff}, which falls between the high-frequency and static dielectric constants $\varepsilon_\infty < \varepsilon_{\text{eff}} < \varepsilon_s$. The second one is that the dielectric screening of the exciton may, in fact, differ between the exciton ground and excited states due to their different radii[39] and, consequently, binding energies, such that the energy spectrum of excited exciton states may not conform to the classic Rydberg series that is predicted by hydrogen-like models (which assume a constant ε_{eff}). Note that the exciton spectra also can differ from the Rydberg series in semiconductors with complex band structure.[40–42] Although, in the lead halide perovskites, the top valence and bottom conduction bands have a simple structure[43,44] (see also Figure S1a, Supporting Information), making the hydrogenic model a good approximation at first glance.

In this study we check the applicability of the Rydberg formula for excitons in $CsPbBr_3$ and determine fundamental exciton parameters such as Rydberg energy, reduced mass, and effective dielectric constant. The reflectivity of light in the optical range of the exciton ground state in high magnetic fields up to 60 T is measured for two circular polarizations of incident light. We modeled the measured spectra within the exciton-polariton model, allowing us to determine with a high accuracy the positions of transverse and longitudinal excitons (TEs and LEs) and their energy splitting, *g*-factors, and diamagnetic shift. To make the evaluation of exciton parameters more accurate, the excited 2P exciton state has also been measured by two-photon excitation in magnetic fields up to 10 T.

2. Results

The sample under study is a fully inorganic lead halide perovskite bulk crystal of $CsPbBr_3$ grown in solution (Experimental Section). Information on its optical and spin properties in low magnetic fields can be found in refs. [44–46]. Here we focus on exciton-polariton parameters and their modification in strong magnetic fields. Experiments were performed at $T = 1.6$ K, with the sample immersed in pumped liquid helium.

It has been appreciated for decades[19,20,47,48] that a proper description of excitons interacting with light in semiconductors requires consideration of the exciton-polariton effect, which accounts for the interaction of the so-called "mechanical exciton" (i.e., the TE) with the light wave. This effect characterizes the dependence of the dielectric function on the wave vector (spatial dispersion) and gives rise to two exciton-polariton modes, which modifies the optical properties of the semiconductor in the spectral range of the exciton-polariton resonance. The splitting between transverse and longitudinal (with respect to the wave vector) excitons is the consequence of the long-range part of the exchange interaction[48] and, simultaneously, is connected with the exciton polarizability, describing its oscillator strength and playing the key role in exciton-polariton dispersion relation. Here we analyze the optical reflectivity of $CsPbBr_3$ crystals in the context of the exciton-polariton model and derive fundamental optoelectronic parameters.

2.1. Reflectivity of Exciton-Polaritons in Pulsed Magnetic Fields

The reflectivity spectrum of the $CsPbBr_3$ crystal at zero magnetic field is shown in **Figure 1**a. It has a pronounced exciton-polariton resonance, which results from the interaction of the mechanical excitons with the photons and their conversion to each other in the crystal. For its model description and fit of the reflectivity spectrum, we used the commonly accepted theory of exciton-polaritons,[20,47] see S2, Supporting Information. For the boundary conditions, we took the "dead" layer approach introduced by Hopfield and Thomas.[47] It is the simplest boundary condition assuming the existence of the finite thickness layer at the edge of the sample, where no excitons are allowed. The thickness of the "dead" layer we treat as a fitting parameter and its value is expected to be of the same order of magnitude as an

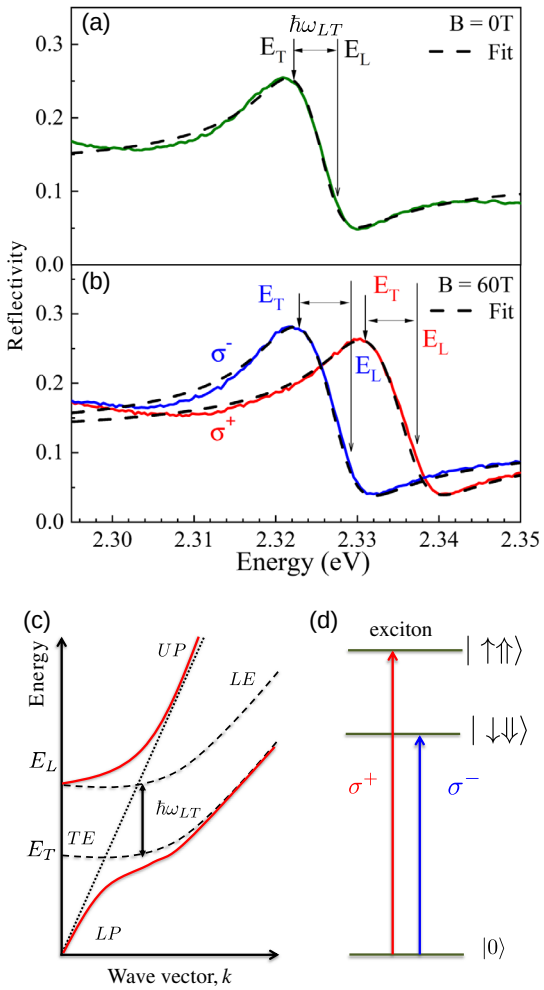

Figure 1. Reflectivity spectra of $CsPbBr_3$ in a) zero and b) 60 T magnetic field, measured at $T = 1.6$ K. Solid lines are experiment and dashed lines are fits. For $B = 0$ T we used TE energy $E_T = 2.322$ eV, longitudinal–transverse splitting $\hbar\omega_{LT} = 5.3$ meV, exciton damping $\hbar\Gamma = 6.7$ meV, and "dead" layer thickness $L = 2.3$ nm. c) Scheme of the exciton–polariton dispersion that accounts for the spatial dispersion. d) Scheme of the exciton optical transitions in magnetic field. Single and double arrows correspond to electron and hole spins, respectively, which in optically active exciton states have spin $+1$ for $|\uparrow\Uparrow\rangle$ and -1 for $|\downarrow\Downarrow\rangle$. $|0\rangle$ is the ground state of the unexcited crystal.

exciton radius. Schematically the exciton-polariton dispersion is shown in Figure 1c. Here, E_T is the energy of the transverse ("mechanical") exciton, E_L is the energy of the LE, and $\hbar\omega_{LT} = E_L - E_T$ is the longitudinal–transverse splitting, which characterizes the exciton oscillator strength.[49] In Figure 1c, "LP" and "UP" denote lower and upper exciton-polariton branches, dashed line "LE" corresponds to longitudinal exciton, dashed line "TE" to transverse exciton without account of the polariton effect; dotted line shows light dispersion. In cubic crystals, LEs are optically inactive and at zero wave vector, their energy coincides with the upper polariton branch.[48,50] Although, $CsPbBr_3$ in low temperatures is in the orthorombic phase, which has a lower symmetry than cubic, and, in principle, LE may be observable in optics, in experiment we do not see any line that can be attributed to LE.

The dashed line in Figure 1a shows the fit of the experimental reflectivity spectrum with Equation (S4), Supporting Information. Here we took the background dielectric constant $\varepsilon_b = 4.3$[51] as a high-frequency one and the translation exciton mass $M = 0.72m_0$. Note that the fit does not depend strongly on the value of M. For details, see S2, Supporting Information. The best fit provides the following exciton-polariton parameters: $E_T = 2.322$ eV, $\hbar\omega_{LT} = 5.3$ meV, exciton damping $\hbar\Gamma = 6.7$ meV, and "dead" layer thickness $L = 2.3$ nm. As it was shown in ref. [47] and can be seen in Figure 1a,b, the TE energy, E_T, does not exactly coincide with the maximum of reflectivity spectrum. We obtain exciton parameters, including E_T and $\hbar\omega_{LT}$, from the fitting of the experimental spectra. Details of the evaluation of the exciton parameters can be found in S2, Supporting Information. We note the considerable value of $\hbar\omega_{LT}$, which justifies the account of the exciton-polariton effect in modeling the reflectivity spectra of $CsPbBr_3$.

Reflectivity spectra were measured in pulsed magnetic fields up to 60 T in σ^+ and σ^- circular polarizations in order to distinguish exciton states with spin ±1 and evaluate the exciton Zeeman splitting and its Landé g-factor (see scheme in Figure 1d). The spectra measured in $B = 60$ T are shown in Figure 1b. One can see the pronounced Zeeman splitting of the oppositely polarized exciton resonances.

There are three effects of magnetic fields on the exciton resonance that we measured and analyzed: the diamagnetic energy shift (which is same for both spin components), the Zeeman splitting, and the increase of the exciton oscillator strength. In the regime of weak magnetic fields, where the exciton binding energy exceeds the cyclotron energies of the electrons and holes, the energy of the n-th exciton state in the hydrogen-like model is

$$E_X^{(n)} = E_g - \frac{R^*}{n^2} \pm \frac{1}{2} g_X \mu_B B + c_d^{(n)} B^2 \tag{1}$$

Here E_g is the free-particle bandgap energy, g_X the exciton Landé g-factor, and μ_B is the Bohr magneton. Here, the plus sign in the Zeeman term $\pm\frac{1}{2} g_X \mu_B B$ corresponds to excitons optically active in σ^+ polarization and the minus sign corresponds to excitons active in σ^-. R^* is the exciton Rydberg, which is equal to the binding energy of a 1S hydrogen-like exciton ground state E_b^{1S}.

$$R^* = E_b^{1S} = \frac{\mu e^4}{2\hbar^2 \varepsilon_{eff}^2} = \frac{e^2}{2\varepsilon_{eff} a_B} \tag{2}$$

where μ is the reduced exciton mass, which is composed of the electron and hole effective masses as $\mu^{-1} = m_e^{-1} + m_h^{-1}$, e is the electron charge, $\hbar$ is the Planck constant, ε_{eff} is the effective dielectric constant, and a_B is the exciton Bohr radius.

$$a_B = \frac{\hbar^2 \varepsilon_{eff}}{\mu e^2} \tag{3}$$

The diamagnetic coefficient $c_d^{(n)}$ is given by

$$c_d^{(n)} = \frac{e^2}{8\mu c^2} \langle \rho_n^2 \rangle \tag{4}$$

where c is speed of light and $\langle \rho_n^2 \rangle$ is the mean square of exciton wave function size in the plane perpendicular to the magnetic field. In the hydrogen-like model for the 1S state, $\langle \rho_{1S}^2 \rangle = 2a_B^2$ and for the $2P_{10}$-state $\langle \rho_{2P}^2 \rangle = 12a_B^2$. The binding energy of the 2P state is four times smaller than the binding energy of the 1S state.

$$E_b^{2P} = \frac{\mu e^4}{8\hbar^2 \varepsilon_{eff}^2} = \frac{e^2}{8\varepsilon_{eff} a_B} \tag{5}$$

We fit the reflectivity spectra measured at all magnetic fields and plot the field dependence of the exciton parameters in **Figure 2**. Figure 2a shows the E_T and E_L energies of the exciton states active in σ^+ and σ^- circular polarizations. The energy of E_L we calculate as $E_L = E_T + \hbar\omega_{LT}$. The Zeeman splitting of the exciton states calculated as $E_{\sigma^+} - E_{\sigma^-} = g_X \mu_B B$ is shown in Figure 2b. The dependences coincide for the E_T and E_L excitons, and their linear fit gives the exciton g-factor $g_X = +2.35$. We emphasize that it is a direct measurement of g_X value and sign, which is positive. This result is in agreement with our recent reports on the universal dependence of exciton[46] and isolated charge carrier[44] g-factors on the bandgap energy in lead halide perovskite bulk crystals. Note that the high linearity of the field dependence of the Zeeman splitting indicates that band mixing is negligibly small in lead halide perovskites even in very strong magnetic fields. This is explained by the simple spin structure (spin 1/2) of the electron and hole bands in the vicinity of the bandgap (which contribute primarily to the exciton wave function) and the rather large energy separation to the higher-lying conduction bands.

The diamagnetic shift of the transverse and LEs, which was calculated as the center of gravity of the $\sigma^{\pm}$ components, is shown in Figure 2c as a function of the square of magnetic field. Dashed lines are B^2 fits; they describe well the experimental data in fields up to 25 T (more details will be given in Figure 4). From the fits we evaluate the diamagnetic coefficients for the TE $c_d^{1S} = 1.6\,\mu eV\,T^{-2}$ and LE $c_d^{L} = 2\,\mu eV\,T^{-2}$. Their difference originates from the increase of the exciton oscillator strength ($\hbar\omega_{LT}$) with magnetic field, which is shown in Figure 2d. It increases from 5.3 meV at zero field up to 6.4 meV at $B = 60$ T. The exciton damping $\hbar\Gamma$ does not significantly depend on the magnetic field (not shown here).

2.2. Two-Photon Spectroscopy of 2P Exciton State

Information about excited exciton states enriches the knowledge of the exciton parameters and allows one to define them with higher precision. Unfortunately, the 2S exciton state was not detectable in reflectivity spectra even in strong magnetic fields, most probably due to its small oscillator strength. Therefore, we used another approach and measured the 2P exciton state, which is forbidden for one-photon excitation, but is allowed for two-photon excitation. We measured the photoluminescence excitation (PLE) spectrum using two-photon excitation, that is,

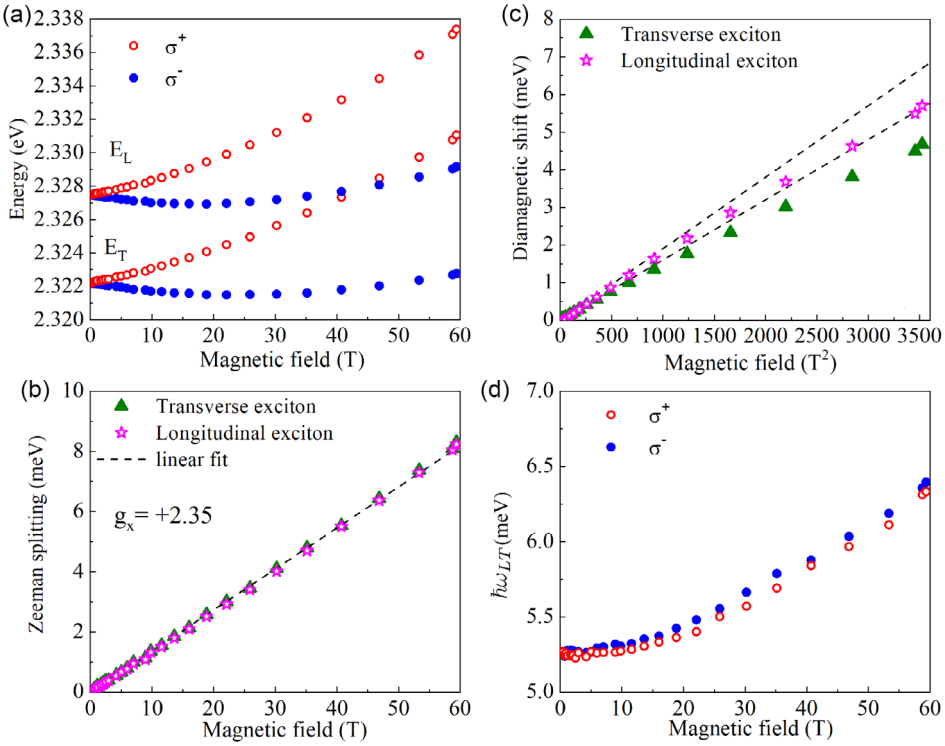

Figure 2. Parameters of the 1S exciton-polariton in $CsPbBr_3$ in strong magnetic fields evaluated from polarized reflectivity spectra. $T = 1.6$ K. a) Energies of transverse (E_T) and longitudinal (E_L) excitons active in σ^+ and σ^- circular polarization as a function of magnetic field. b) Magnetic field dependence of the Zeeman splitting $E_{\sigma^+} - E_{\sigma^-}$ of transverse (triangles) and longitudinal (open stars) excitons. The dashed line is a linear fit with $g_X = +2.35$. c) Diamagnetic shift of transverse and LE versus B^2. Dashed lines are B^2 fits with $c_d^{1S} = 1.6\,\mu eV\,T^{-2}$ and $c_d^{L} = 2\,\mu eV\,T^{-2}$, respectively. d) The longitudinal–transverse splitting in two circular polarizations as a function of magnetic field.

the laser photon energy was tuned in the range close to $E_g/2$. Recently, we used this technique to study excitons in CdSe colloidal nanoplatelets.[52]

Figure 3 shows the two-photon PLE spectra of $CsPbBr_3$ measured in zero magnetic field and in 10 T. One can see a pronounced resonance of the 2P exciton with a maximum at $E_{2P} = 2.3467$ eV at zero magnetic field. At $B = 10$ T, the maximum is shifted to 2.3476 eV. The diamagnetic shift of the 2P state is shown in the inset of Figure 3. The red line shows a B^2 fit using the diamagnetic coefficient $c_d^{2P} = 10\,\mu eV\,T^{-2}$. Note that this state corresponds to the $2P_{10}$ state with $m = 1$ (orbital momentum) and $q = 0$ (its projection on the light wave vector) following ref. [53], where magnetoexciton states are calculated within a hydrogen-like model.

2.3. Evaluation of Exciton Parameters

We now turn to the evaluation of the fundamental exciton parameters, which control its ground and excited Rydberg states: binding energy, reduced mass, and effective dielectric constant. There are several challenges involved. Firsty, the most straightforward way to measure the exciton Rydberg energy, that is, the binding energy of its 1S state, would be to measure it as $R^* = E_g - E_T$. But in the studied $CsPbBr_3$ crystal, similar to other lead halide perovskite crystals and polycrystalline films,[31,34] the free-particle gap E_g has no pronounced feature in optical spectra. It can, in principle, be evaluated by different means, such as by extrapolation to zero field of the magneto-exciton fan chart measured in strong magnetic fields, but the accuracy of this approach is limited. In ref. [31], the 1S exciton ground-state binding energy was measured by comparing the energy positions of 1S and 2S exciton states. However, the latter was pronounced only in high magnetic fields and its position in zero field was extrapolated. Secondly, as already mentioned, in lead halide perovskites the screening of the Coulomb interaction may be different for different exciton states, and consequently exciton energies can deviate from the standard hydrogenic Rydberg series.

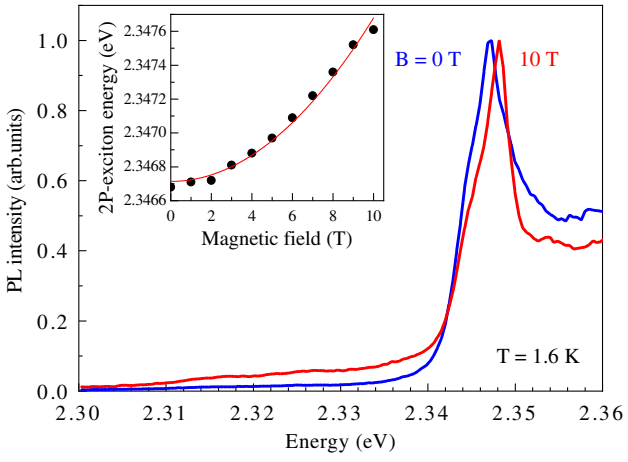

Figure 3. Two-photon PLE spectra of $CsPbBr_3$ in zero magnetic field and in 10 T. The PL detection energy is 2.30 eV. Inset: the magnetic field dependence of the 2P exciton energy. Symbols are experimental data. B^2 fit with diamagnetic coefficient $c_d^{2P} = 10\,\mu eV\,T^{-2}$ is shown by the red line.

One approach to estimate the deviation of the binding energies of the exciton states from the hydrogen-like model is based on comparison of the diamagnetic coefficients for the 1S and 2P states. The hydrogen-like model predicts a ratio $c_d^{1S}/c_d^{2P} = 1/6$; see ref. [53] and Equation (8) and (9). The experimental values that we obtained here are $c_d^{1S} = 1.6\,\mu eV\,T^{-2}$ and $c_d^{2P} = 10\,\mu eV\,T^{-2}$. Their ratio is 1/6.25, which evidences the good validity of the hydrogen-like model for describing excitons in $CsPbBr_3$.

For accurate and self-consistent evaluation of the exciton parameters, we treat the effective dielectric constant ε_{eff} for 1S (ε_{1S}) and 2P (ε_{2P}) exciton states as independent fitting parameters and determine them separately from the analysis of the experimental data, see S2, Supporting Information, for details. We have four parameters to be determined: the exciton reduced mass (μ), the bandgap energy (E_g), and the effective dielectric constants for the 1S and 2P states (ε_{1S} and ε_{2P}). We use, therefore, four experimentally measured values: the diamagnetic coefficients (c_d^{1S} and c_d^{2P}) and exciton resonance energies ($E^{1S} = E_T$, and E^{2P}). We use the four following equations, which link the evaluated and measured parameters.

$$E^{1S} = E_g - E_b^{1S} = E_g - \frac{e^4}{2\hbar^2}\frac{\mu}{\varepsilon_{1S}^2} \tag{6}$$

$$E^{2P} = E_g - E_b^{2P} = E_g - \frac{e^4}{8\hbar^2}\frac{\mu}{\varepsilon_{2P}^2} \tag{7}$$

$$c_d^{1S} = \frac{\hbar^4}{4e^2c^2}\frac{\varepsilon_{1S}^2}{\mu^3} \tag{8}$$

$$c_d^{2P} = \frac{3\hbar^4}{2e^2c^2}\frac{\varepsilon_{2P}^2}{\mu^3} \tag{9}$$

An equal number of evaluated parameters and linear equations provides accurate and unequivocal evaluation of all parameters. The following parameters are determined: $\mu = 0.18m_0$, $E_g = 2.3545$ eV, $\varepsilon_{1S} = 8.66$, and $\varepsilon_{2P} = 8.84$. They bring us to the exciton binding energies of $E_b^{1S} = 32.5$ meV and $E_b^{2P} = 7.8$ meV for the 1S and 2P states, respectively. Note that the values of ε_{1S} and ε_{2P} are quite close; therefore, it is safe to assume that all the exciton states can be treated within the hydrogen-like model with a single effective dielectric constant $\varepsilon_{eff} \approx 8.7$ with reasonable accuracy. Moreover, the ratio $E_b^{1S}/E_b^{2P} \approx 4.17$ is close to the value of 4 that is predicted by the hydrogen-like model (Equation (2) and (5)). From Equation (3), we get the Bohr radius of the 1S state $a_B^{1S} = 2.55$ nm.

In **Table 1** we summarize the parameters measured and evaluated in this work, and further details are given in Table S2, Supporting Information.

3. Discussion

Let us have a close look at the field-dependent energy shift of the 1S exciton state, plotted in Figure 2c as a function of B^2 and also in **Figure 4** as a function of B. In both cases one can see that the pure B^2 shift is valid primarily in magnetic fields weaker than

Table 1. Exciton parameters in bulk $CsPbBr_3$ single crystal. $T = 1.6$ K.

Parameter	Value	Comments
$E_T = E^{1S}$	2.3220 eV	Energy of TE
E_L	2.3273 eV	Energy of LE.
$\hbar\omega_{LT}$	5.3 meV	Longitudinal–transverse splitting.
$\hbar\Gamma$	6.7 meV	Exciton damping.
$4\pi\alpha_0$	0.0195	Exciton polarizability.
ε_b	4.3	Background dielectric constant. Taken as $\varepsilon_b = \varepsilon_\infty = 4.3$ from ref. [51].
E^{2P}	2.3467 eV	Energy of the 2P exciton.
g_X	+2.35	Exciton g-factor.
c_d^{1S}	1.6 μeV T^{-2}	Diamagnetic coefficient of 1S exciton.
c_d^{2P}	10 μeV T^{-2}	Diamagnetic coefficient of 2P exciton.
E_b^{1S}	32.5 meV	Binding energy of the 1S exciton state, that is, the exciton Rydberg R^* in hydrogen-like model.
E_b^{2P}	7.8 meV	Binding energy of the 2P exciton state.
E_g	2.3545 eV	Bandgap energy.
ε_{eff}	8.7	Effective dielectric constant.
μ	$0.18m_0$	Reduced exciton mass.
M	$0.72m_0$	Translation exciton mass.
a_B^{1S}	2.55 nm	Bohr radius of the exciton ground state.

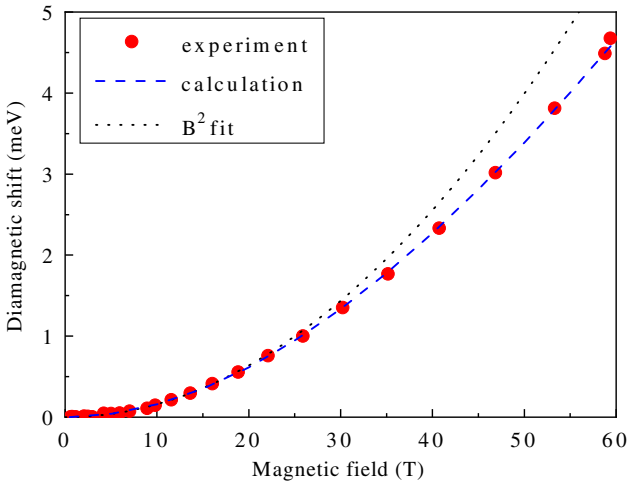

Figure 4. The 1S exciton shift in magnetic field measured (circles), calculated with Equation (10) (dashed line) and B^2 fit (dotted line). $\mu = 0.18m_0$ and $\varepsilon_{eff} = 8.7$.

25 T. Here, the condition for the diamagnetic exciton is fulfilled with high accuracy. Namely, the cyclotron radius of the charge carriers $\sqrt{c\hbar/eB}$ should be larger than the exciton Bohr radius a_B. The critical magnetic field for this criterion is $B_c = c\hbar/(ea_B^2)$. In $CsPbBr_3$ it gives $B_c \approx 100$ T, which is only a factor of ≈2 larger than the 60 T fields we use. Therefore we can expect a small deviation from purely quadratic diamagnetic shifts when approaching the high fields used in this work.

The dashed line in Figure 4 shows the results of a full calculation that accounts for the decrease of the exciton radius in strong magnetic fields. This simple model Hamiltonian neglects the motion of the exciton center of mass.

$$\hat{H} = \frac{\hbar^2}{2\mu}\Delta - \frac{e^2}{\varepsilon_{eff} r} + \frac{1}{8}\frac{e^2}{c^2}\frac{B^2}{\mu}(x^2 + y^2) \tag{10}$$

Here Δ is the Laplace operator, acting on the electron and hole relative coordinate r, and x and y are components of r in the plane perpendicular to the magnetic field. Equation (10) was solved numerically. We used values of $\mu = 0.18m_0$ and $\varepsilon_{eff} \approx 8.7$ that were determined above. Note that the received exciton diamagnetic shift deviates from the B^2 fit in magnetic fields exceeding 20 T. One can see an excellent agreement with experiment in the whole range of measured magnetic fields, which justifies our assumptions made for the calculation of exciton parameters and shows the consistency of the obtained set of exciton parameters.

The exciton parameters measured in this study allow us to estimate the Kane energy E_p, which is connected with the interband momentum matrix element P_{cv} as $E_p = 2P_{cv}^2/m_0$. The Kane energy characterizes the efficiency of the light interaction with the crystal, for details, see S3, Supporting Information.[44,54,55] We have two ways to do that. In the first approach, we estimate E_p from the electron and hole effective masses.[44,55] In lead halide perovskites the electron and hole effective masses are similar.[56] Therefore, we estimate $m_h = 2\mu$, which for $\mu = 0.18m_0$ gives $m_h = 0.36m_0$. Then taking the bandgap energy of $CsPbBr_3$ of $E_g = 2.35$ eV and the conduction band spin-orbit splitting $\Delta_{SO} = 1.5$ eV[44] we get from Equation (S13), Supporting Information, $E_p = 11.8$–12.5 eV. The two values result from evaluations via the electron and hole effective masses.

We made a second evaluation of E_p from the link between the longitudinal–transverse splitting and E_p given by[24]

$$\hbar\omega_{LT} = \frac{4e^2\hbar^2}{3m_0 E_T^2}\frac{E_p}{\varepsilon_b a_B^3} \tag{11}$$

Using parameters from Table 1, we calculate $E_p = 15$ eV, which is close to the value from the first evaluation. This agreement justifies use of the exciton–polariton approach and obtained exciton parameters. Note that due to the difference of the band structure of the lead halide perovskites and conventional zinc-blende semiconductors, for the latter in Equation (11), coefficient 2 should be used instead of 4/3.

The following evaluations of E_p can be made on the basis of literature data. In ref. [44] the effective masses of electrons and holes were calculated by density functional theory (DFT) and empirical tight-binding (ETB) methods, the reported values are $m_e = 0.3(0.291)m_0$ and $m_h = 0.26(0.298m_0)$ for DFT (ETB), respectively. Also the experimental value for hole effective mass $m_h = 0.26m_0$ was measured by angle-resolved photoelectron spectroscopy in ref. [5]. They correspond to a reduced exciton mass $\mu = 0.14$–0.15 and a Kane energy $E_p = 13.5 - 17.5$ eV. In ref. [44], from the modeling of the universal dependence of the charge carrier g-factors on the bandgap energy, the parameter $P_{cv} = \hbar p/m_0 = 6.8$ eVÅ was evaluated. It corresponds to a Kane energy $E_p = 12.1$ eV.

Magneto-optical experiments in high fields up to 70 T were reported for $CsPbBr_3$ polycrystalline films in ref. [31]. The following exciton parameters were evaluated: $R^* = E_b^{1S} = 33 \pm 1$ meV,

$\mu = (0.126 \pm 0.01)m_0$, and $\varepsilon_{\text{eff}} = 7.8$. The exciton binding energy of the 1S state, estimated as the difference between the energy of the 1S exciton and extrapolation of the magneto-exciton fan chart to get E_g, is very close to our value of 32.5 meV. While the reduced exciton mass, evaluated from the fit of the fan chart in strong magnetic fields, is smaller than our determination of $\mu = 0.18m_0$, which is based on diamagnetic shifts in fields below 25 T, it can be measured with high accuracy due to the narrow exciton lines in bulk crystals. ε_{eff} evaluated in ref. [31] from E_b^{1S} and μ is smaller than our value of 8.7, which is related to the smaller μ value. The bandgap energy of $E_g = 2.3545$ eV that we determine in our study is in line with the literature data.[6,31,57]

4. Conclusion

Magneto-optics and two-photon spectroscopy of $CsPbBr_3$ crystals allow us to determine a detailed set of exciton and exciton-polariton parameters summarized in Table 1. The combination of these approaches can be readily extended to other lead halide perovskites and their nanostructures.

5. Experimental Section

Samples: The $CsPbBr_3$ crystals were grown with a slight modification of the inverse temperature crystallization technique, see ref. [58]. First, CsBr and $PbBr_2$ were dissolved in dimethyl sulfoxide. Afterward, a cyclohexanol in N,N-dimethylformamide solution was added. The resulting mixture was heated in an oil bath to 105 °C whereby slow crystal growth occured. The obtained crystals were taken out of the solution and quickly loaded into a vessel with hot (100 °C) N,N-dimethylformamide. Once loaded, the vessel was slowly cooled down to about 50 °C. After that, the crystals were isolated, wiped with filter paper, and dried. The obtained rectangular-shaped $CsPbBr_3$ was crystallized in the orthorhombic modification. The crystals had one selected (long) side along the *c*-axis [001] and two nearly identical sides along the $[\bar{1}10]$ and [110] axes.[59]

Reflectivity in Pulsed Magnetic Fields: The sample was mounted on a custom fiber-coupled probe in a helium bath cryostat with a long tail extending into the bore of a 65 T pulsed magnet. The experiments were performed at $T = 1.6$ K, with the sample immersed in superfluid helium. Broadband white light from a halogen lamp was coupled down a 100 µm-diameter multimode optical fiber, and light reflected from the sample was collected by a 600 µm-diameter fiber. The light wavevector **k** was perpendicular to the sample surface and parallel to *B* (Faraday geometry). Thin-film circular polarizers were used to select σ^- and σ^+ polarized light. Full optical spectra were acquired every 1 ms continuously throughout the magnet pulse using a fast charge-coupled-device camera combined with a 0.3 m spectrometer. To switch between σ^- and σ^+ polarization, the direction of the magnetic field was switched. Further details of these methods can be found in ref. [60].

Two-Photon Excitation of Photoluminescence: In order to obtain information on the energy of the 2 P exciton state in absorption, we measured PLE spectra. In this technique the emission was detected at the low energy tail of the PL spectrum and the laser photon energy was tuned across the exciton absorption spectral range. For excitation, a pulsed laser system with an optical parametric amplifier was used. Its photon energy was tunable in the spectral range of 0.5–4.0 eV. The laser pulses had a duration of 2.5 ps, a linewidth of 0.23 nm, and a repetition frequency of 30 kHz. For the two-photon PLE, the laser was tuned in the range of 1.15–1.20 eV. The PL was measured at 2.30 eV, about 50 meV below the exciton energy. For this, it was spectrally selected by a 10 nm-wide bandpass filter and a spectrometer. For these measurements the sample was placed in the magneto-optical cryostat with direct optical access. The sample was in direct contact with pumped liquid helium at $T = 1.6$ K. Static magnetic fields up to 10 T were generated by a split-coil superconducting magnet and applied in the Faraday geometry.

Supporting Information

Supporting Information is available from the Wiley Online Library or from the author.

Acknowledgements

The authors are thankful to M. M. Glazov and E. L. Ivchenko for fruitful discussions and to P. Sercel for valuable advice. The authors acknowledge financial support of the Deutsche Forschungsgemeinschaft through the Collaborative Research Center TRR142 (Project A11) and the Priority Programme SPP2196 (Project YA 65/26-1). M.A.S. acknowledges support of the Russian Science Foundation (project 23-12-00300). The National High Magnetic Field Laboratory is supported by the National Science Foundation DMR-1644779, the State of Florida, and the US Department of Energy. S.A.C. acknowledges support from the US Department of Energy "Science of 100 T" program. Work at ETH Zürich (D.N.D. and M.V.K.) was financially supported by the Swiss National Science Foundation (grant agreement 186406, funded in conjunction with SPP219 through DFG-SNSF bilateral program) and by ETH Zürich through ETH+ Project SynMatLab.

Open Access funding enabled and organized by Projekt DEAL.

Conflict of Interest

The authors declare no conflict of interest.

Data Availability Statement

The data that support the findings of this study are available from the corresponding author upon reasonable request.

Keywords

$CsPbBr_3$, exciton binding energies, exciton-polaritons, high magnetic fields, Landé factors, perovkite semiconductors, two-photon spectroscopies

Received: October 29, 2023
Published online: November 15, 2023

[1] *Hybrid Organic Inorganic Perovskites: Physical Properties and Applications* (Eds: Z. V. Vardeny, M. C. Beard), World Scientific, Singapore **2022**.
[2] *Halide Perovskites for Photonics* (Eds: A. Vinattieri, G. Giorgi), AIP Publishing, Melville, NY **2021**.
[3] Z. Fan, J. Liu, W. Zuo, G. Liu, X. He, K. Luo, Q. Ye, C. Liao, *Phys. Status Solidi A* **2020**, *217*, 2000104.
[4] Z. Zhang, B. Saparov, *Appl. Phys. Lett.* **2021**, *119*, 030502.
[5] M. Puppin, S. Polishchuk, N. Colonna, A. Crepaldi, D. N. Dirin, O. Nazarenko, R. De Gennaro, G. Gatti, S. Roth, T. Barillot, L. Poletto, R. P. Xian, L. Rettig, M. Wolf, R. Ernstorfer, M. V. Kovalenko, N. Marzari, M. Grioni, M. Chergui, *Phys. Rev. Lett.* **2020**, *124*, 206402.
[6] M. Kulbak, D. Cahen, G. Hodes, *J. Phys. Chem. Lett.* **2015**, *6*, 2452.
[7] M. Kulbak, S. Gupta, N. Kedem, I. Levine, T. Bendikov, G. Hodes, D. Cahen, *J. Phys. Chem. Lett.* **2016**, *7*, 167.

[8] J. Song, L. Xu, J. Li, J. Xue, Y. Dong, X. Li, H. Zeng, *Adv. Mater.* **2016**, *28*, 4861.
[9] G. J. Matt, I. Levchuk, J. Knüttel, J. Dallmann, A. Osvet, M. Sytnyk, X. Tang, J. Elia, R. Hock, W. Heiss, C. J. Brabec, *Adv. Mater. Interfaces* **2020**, *7*, 1901575.
[10] C. Stoumpos, C. D. Malliakas, J. A. Peters, Z. Liu, M. Sebastian, J. Im, T. C. Chasapis, A. C. Wibowo, D. Y. Chung, A. J. Freeman, B. W. Wessels, M. G. Kanatzidis, *Cryst. Growth Des.* **2013**, *13*, 2722.
[11] K. Heidrich, H. Künzel, J. Treusch, *Solid State Commun.* **1978**, *25*, 887.
[12] H. Ito, H. Onuki, R. Onaka, *J. Phys. Soc. Jpn.* **1978**, *45*, 2043.
[13] D. Fröhlich, K. Heidrich, H. Künzel, G. Trendel, J. Treusch, *J. Lumin.* **1979**, *18/19*, 385.
[14] K. Heidrich, W. Schäfer, M. Schreiber, J. Söchtig, G. Trendel, J. Treusch, T. Grandke, H. J. Stolz, *Phys. Rev. B* **1981**, *24*, 5642.
[15] R. Su, S. Ghosh, J. Wang, S. Liu, C. Diederichs, T. C. H. Liew, Q. Xiong, *Nat. Phys.* **2020**, *16*, 301.
[16] R. Su, A. Fieramosca, Q. Zhang, H. S. Nguyen, E. Deleporte, Z. Chen, D. Sanvitto, T. C. H. Liew, Q. Xiong, *Nat. Mater.* **2021**, *20*, 1315.
[17] R. Tao, K. Peng, L. Haeberlé, Q. Li, D. Jin, G. R. Fleming, S. Kéna-Cohen, X. Zhang, W. Bao, *Nat. Mater.* **2022**, *21*, 761.
[18] I. Dursun, Y. Zheng, T. Guo, M. De Bastiani, B. Turedi, L. Sinatra, M. A. Haque, B. Sun, A. A. Zhumekenov, M. I. Saidaminov, F. P. García de Arquer, E. H. Sargent, T. Wu, Y. N. Gartstein, O. M. Bakr, O. F. Mohammed, A. V. Malko, *ACS Energy Lett.* **2018**, *3*, 1492.
[19] D. C. Reynolds, T. C. Collings, *Excitons: Their Properties and Uses*, Academic Press, New York, NY **1981**.
[20] C. Klingshirn, *Semiconductor Optics*, Springer-Verlag, Berlin **2005**.
[21] W. Bao, X. Liu, F. Xue, F. Zheng, R. Tao, S. Wang, Y. Xia, M. Zhao, J. Kim, S. Yang, Q. Li, Y. Wang, Y. Wang, L.-W. Wang, A. H. MacDonald, X. Zhang, *PNAS* **2019**, *116*, 20274.
[22] R. P. Seisyan, B. P. Zakharchenya, in *Landau Level Spectroscopy* (Eds: G. Landwehr, E. I. Rashba), Elsevier Science Publishers B.V., Amsterdam **1991**, pp. 347–443.
[23] R. P. Seisyan, *Semicond. Sci. Technol.* **2012**, *27*, 053001.
[24] E. L. Ivchenko, *Optical Spectroscopy of Semiconductor Nanostructures*, Springer, Berlin **2007**.
[25] T. Kataoka, T. Kondo, R. Ito, S. Sasaki, K. Uchida, N. Miura, *Phys. Rev. B* **1993**, *47*, 2010.
[26] M. Hirasawa, T. Ishihara, T. Goto, K. Uchida, N. Miura, *Physica B* **1994**, *201*, 427.
[27] K. Tanaka, T. Takahashi, T. Ban, T. Kondo, K. Uchida, N. Miura, *Solid State Commun.* **2003**, *127*, 619.
[28] K. Tanaka, T. Takahashi, T. Kondo, K. Umeda, K. Ema, T. Umebayashi, K. Asai, K. Uchida, N. Miura, *Jpn. J. Appl. Phys.* **2005**, *44*, 5923.
[29] A. Miyata, A. Mitioglu, P. Plochocka, O. Portugall, J. Tse-Wei Wang, S. D. Stranks, H. J. Snaith, R. J. Nicholas, *Nat. Phys.* **2015**, *11*, 582.
[30] K. Galkowski, A. Mitioglu, A. Miyata, P. Plochocka, O. Portugall, G. E. Eperon, J. T.-W. Wang, T. Stergiopoulos, S. D. Stranks, H. J. Snaith, R. J. Nicholas, *Energy Environ. Sci.* **2016**, *9*, 962.
[31] Z. Yang, A. Surrente, K. Galkowski, A. Miyata, O. Portugall, R. J. Sutton, A. A. Haghighirad, H. J. Snaith, D. K. Maude, P. Plochocka, R. J. Nicholas, *ACS Energy Lett.* **2017**, *2*, 1621.
[32] Z. Yang, A. Surrente, K. Galkowski, N. Bruyant, D. K. Maude, A. A. Haghighirad, H. J. Snaith, P. Plochocka, R. J. Nicholas, *J. Phys. Chem. Lett.* **2017**, *8*, 1851.
[33] M. Baranowski, P. Plochocka, R. Su, L. Legrand, T. Barisien, F. Bernardot, Q. Xiong, C. Testelin, M. Chamarro, *Photonics Res.* **2020**, *8*, A50.
[34] M. Baranowski, P. Plochocka, *Adv. Mater.* **2020**, *10*, 1903659.
[35] M. Baranowski, K. Galkowski, A. Surrente, J. Urban, Ł. Kłopotowski, S. Maćkowski, D. K. Maude, R. Ben Aich, K. Boujdaria, M. Chamarro, C. Testelin, P. K. Nayak, M. Dollmann, H. J. Snaith, R. J. Nicholas, P. Plochocka, *Nano Lett.* **2019**, *19*, 7054.
[36] I. P. Pashuk, N. S. Pidzyrailo, M. G. Matsko, *Sov. Phys. Solid State* **1981**, *23*, 1263.
[37] X. Zhou, Z. Zhang, *AIP Adv.* **2020**, *10*, 125015.
[38] Y. Guo, O. Yaffe, T. D. Hull, J. S. Owen, D. R. Reichman, L. E. Brus, *Nat. Commun.* **2019**, *10*, 1175.
[39] A. Franceschetti, L. W. Wang, H. Fu, A. Zunger, *Phys. Rev. B* **1998**, *58*, R13367.
[40] A. Baldereschi, N. O. Lipari, *Phys. Rev. B* **1971**, *3*, 439.
[41] A. Baldereschi, N. O. Lipari, *Phys. Rev. B* **1973**, *8*, 2697.
[42] A. Baldereschi, N. O. Lipari, *Phys. Rev. B* **1974**, *9*, 1525.
[43] J. Even, L. Pedesseau, M.-A. Dupertuis, J.-M. Jancu, C. Katan, *Phys. Rev. B* **2012**, *86*, 205301.
[44] E. Kirstein, D. R. Yakovlev, M. M. Glazov, E. A. Zhukov, D. Kudlacik, I. V. Kalitukha, V. F. Sapega, G. S. Dimitriev, M. A. Semina, M. O. Nestoklon, E. L. Ivchenko, N. E. Kopteva, D. N. Dirin, O. Nazarenko, M. V. Kovalenko, A. Baumann, J. Höcker, V. Dyakonov, M. Bayer, *Nat. Commun.* **2022**, *13*, 3062.
[45] V. V. Belykh, D. R. Yakovlev, M. M. Glazov, P. S. Grigoryev, M. Hussain, J. Rautert, D. N. Dirin, M. V. Kovalenko, M. Bayer, *Nat. Commun.* **2019**, *10*, 673.
[46] N. E. Kopteva, D. R. Yakovlev, E. Kirstein, E. A. Zhukov, D. Kudlacik, I. V. Kalitukha, V. F. Sapega, O. Hordiichuk, D. N. Dirin, M. V. Kovalenko, A. Baumann, J. Höcker, V. Dyakonov, S. A. Crooker, M. Bayer, https://doi.org/10.48550/arXiv.2301.12775 (accessed: January 2023).
[47] J. J. Hopfield, D. G. Thomas, *Phys. Rev.* **1963**, *132*, 563.
[48] L. C. Andreani, F. Bassani, A. Quattropani, *il Nuovo Cimento D* **1988**, *10*, 1473.
[49] M. M. Denisov, V. P. Makarov, *Phys. Status Solidi B* **1973**, *56*, 9.
[50] J. J. Hopfield, D. G. Thomas, *J. Phys. Chem. Solids* **1960**, *12*, 276.
[51] K. Miyata, D. Meggiolaro, M. T. Trinh, P. P. Joshi, E. Mosconi, S. C. Jones, F. De Angelis, X.-Y. Zhu, *Sci. Adv.* **2017**, *3*, 1701217.
[52] E. V. Shornikova, D. R. Yakovlev, N. A. Gippius, G. Qiang, B. Dubertret, A. H. Khan, A. Di Giacomo, I. Moreels, M. Bayer, *Nano Lett.* **2021**, *21*, 10525.
[53] P. C. Makado, N. C. McGill, *J. Phys. C: Solid State Phys.* **1986**, *19*, 873.
[54] E. O. Kane, *J. Phys. Chem. Solids* **1957**, *1*, 249.
[55] Z. G. Yu, *Sci. Rep.* **2016**, *6*, 28576.
[56] M. A. Becker, R. Vaxenburg, G. Nedelcu, P. C. Sercel, A. Shabaev, M. J. Mehl, J. G. Michopoulos, S. G. Lambrakos, N. Bernstein, J. L. Lyons, T. Stöferle, R. F. Mahrt, M. V. Kovalenko, D. J. Norris, G. Rain, A. L. Efros, *Nature* **2018**, *553*, 189. In Supporting Information.
[57] J. B. Hoffman, A. L. Schleper, P. V. Kamat, *J. Am. Chem. Soc.* **2016**, *138*, 8603.
[58] D. N. Dirin, I. Cherniukh, S. Yakunin, Y. Shynkarenko, M. V. Kovalenko, *Chem. Mater.* **2016**, *28*, 8470.
[59] Y. Feng, L. Pan, H. Wei, Y. Liu, Z. Ni, J. Zhao, P. N. Rudd, L. R. Cao, J. Huang, *J. Mater. Chem. C* **2020**, *8*, 11360.
[60] A. V. Stier, K. M. McCreary, B. T. Jonker, J. Kono, S. A. Crooker, *Nat. Commun.* **2016**, *7*, 10643.